EXPERIMENTAL INVESTIGATION INTO THE EFFECT OF CIRCUMFERENTIAL NON-UNIFORM HEAT FLUX ON A CIRCULAR TUBE IN THE LAMINAR FLOW REGIME

Reid W.J., Dirker J.* and Meyer J.P.
*Author for correspondence
Department of Mechanical and Aeronautical Engineering,
University of Pretoria,
Pretoria, 0002,
South Africa,
E-mail: jaco.dirker@up.ac.za

ABSTRACT

In this experimental investigation the influence of buoyancy driven secondary flow on the effective length-wise heat transfer coefficient in a circular horizontal tube is considered for liquid water at different applied external circumferential heat flux distributions. The test section consisted of a 2 m long stainless steel tube with an inner diameter of 27.8 mm and a wall thickness of 2.77 mm. Hydrodynamic fully developed inlet flow at a uniform temperature of approximately 20°C was considered for a Reynolds number range from 650 to 2600. Three externally imposed heat flux distributions were examined: a fully uniform heat flux condition along the length and the circumference of the tube and another two, where only the lower or upper halves of the tube experienced uniform heat flux, while the non-heated halves were externally adiabatic. Results showed that the heat flux distribution had a significant influence on the effective Nusselt number. The fully uniform heat flux distribution cases produced the highest Nusselt numbers. The cases where only the lower half of the tube was heated had higher Nusselt numbers than the cases where only the upper half was heated.

INTRODUCTION

There are a large number of real world cases where heat (energy) exchangers and heat collector tubes do not experience perfectly uniform heat flux. The solar industry is a good example where there is a significant non-uniformity with regards to the incoming heat flux, especially with heliostats or mirrors focusing rays from below receiver tubes. The rapid growth of the solar industry is evident, with the USA having over 25000 CSP (Concentrated Solar Power) plants planned [1]. With the overwhelming increase in solar projects it is imperative that as much information as possible is found to ensure that solar projects are built to be as efficient and cost effective as possible. While most commercial solar power plants are designed to operate solar collectors in the turbulent flow regime to reduce thermal resistances in order to increase the thermal efficiency of the plant, there are other applications which may operate in the laminar flow regime such as thermo syphon driven solar water heating systems. Depending on the solar reflectors, heat may be concentrated from below onto a collector tube.

Often, for high Reynolds number turbulent flow, the well-known Dittus-Boelter equation which was developed for circular tubes, is found to be reasonably accurate for uniform and non-uniform heat flux cases [2]. This is because for most turbulent flow cases, forced convection is dominant and secondary flow does not have a large influence on the heat transfer performance.

However, at lower flow rates, secondary flow may become significant and may result in mixed convection [3]. The impact there-of is dependent on the flow-regime (laminar, transitional or turbulent), the physical orientation of the flow passage and the direction of the primary flow in relation to the secondary flow direction [4]. Due to this, the effect of secondary flow on heat transfer in horizontal pipes with circumferential uniform heat flux has been extensively investigated [5-8]. Depending on the flow conditions, a significant improvement in the heat transfer coefficient can be sustained due to improved mixing mechanism brought about by the induced flow patterns.

Even though research has been performed for uniform heat transfer cases, relatively little investigation has been conducted to characterize the impact of non-uniform heating cases. It has been shown that there is a significant difference in the steady

NOMENCLATURE

C_p	[J/kg·K]	Specific heat
D	[m]	Inner diameter
h	[W/m^{2}K]	Heat transfer coefficient
k	[W/mK]	Thermal conductivity
$\dot{m}$	[kg/s]	Mass flow rate
Nu	[-]	Nusselt number
$\dot{Q}$	[W]	Heat transfer rate
Re	[-]	Reynolds number
T	[˚C]	Temperature

Greek symbols

ρ	[kg/m^3]	Density

Subscripts

B	Bulk
m	Measuring station
in	Inlet / Input
n	Thermocouple position
out	Outlet / Output
w	Wall

state heat transfer and flow fields if, for instance, the upper and lower halves of a circular tube are heated [9]. Intuition indicates that when the lower half is heated stronger secondary flow is produced which would enhance the effective heat transfer coefficient, which is technically also the case. However, based on the current state of literature, not enough numerical or experimental data is available in order to quantify the effect of non-uniformity of the heat source. For this reason the purpose of this study is to produce experimental data which can be used to describe the influence of the heat flux distribution around a horizontal circular tube on the effective heat transfer coefficient.

EXPERIMENTAL SETUP

Test Facility

Figure 1 gives a representation of the test facility. It consisted of a closed water loop which was equipped with a 1000 L storage tank cooled by a 45 kW chiller unit (item 7). A pump (item 8) was used to circulate the water through the test line and the bypass line. An accumulator (item 3) was used to reduce flow pulsations, while a filter (item 6) was used to prevent small particles from entering the test line which might affect the results. Pressure gauges (items 2a-c) were installed to ensure that the pressure in the system could be monitored. A Coriolis flow meter (item 5) with a measuring range of 0 to 0.604 kg/s and an accuracy of 0.04% (average) was used to determine the water flow rate. Hand-operated ball valves (items 1a-c) and a non-return valve (item 4) were used to isolate sections of the water loop as required The bypass line was used to ensure that a low, stable flow rate through the test line could be achieved. National instruments chassis and data cards which were connected to a desktop PC were used in the data acquisition process.

Test Section

The test section, shown in Figure 2, was placed in the test line and consisted of two main portions. The first portion was an adiabatic 27.8 mm inner diameter stainless steel tube (item 10 in Figure 1) with a wall thickness of 2.77 mm and a length of 3 m which acted as a calming entry length to produce hydrodynamic fully developed flow.

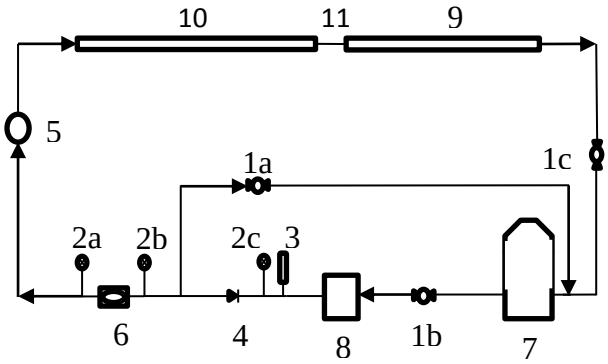

Figure 1 Experimental test setup.

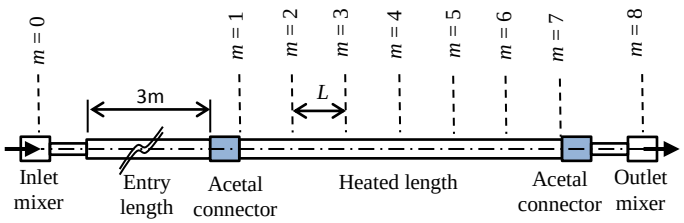

Figure 2 Side view schematic of the test section.

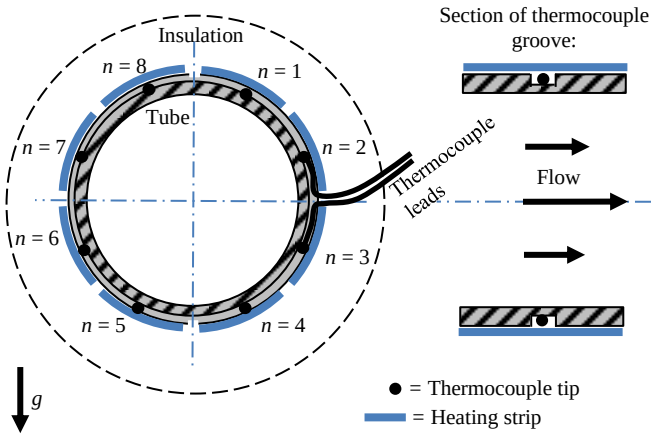

Figure 3 Details for the heated tube portion.

The second portion was an externally heated stainless steel tube (item 9 in Figure 1) which had the same diameter and tube wall thickness as the entry length. Stainless steel with a thermal conductivity of 16.1 W/mK was chosen to ensure minimal circumferential heat conduction in the tube wall. It was thermally insulated from the entry length by an Acetal bush (item 11 in Figure 1) which had an axial length of 130 mm. The second tube portion had a total length of 2.2 m, and was heated by 8 identical 2 m-long heating elements strips ($n = 1$ to $n = 8$) positioned longitudinally around the external circumference (shown in Figure 3). Each heating element strip consisted of a multi-pass constantan heating wire and was directly attached to the outer wall of the tube to ensure good thermal contact with the tube. The gaps between the heating elements seen in Figure 3 are solely to better show the individual heating element strips, in reality there is no space between the strips. Additionally, all heating elements were clamped onto the tube at 10 mm intervals as well as taped down. The elements were powered by a 3 kW DC power supply, with 0 to 360 V, and 0 to 30 A ranges. The power supply and heating elements could be individually controlled to allow for different heating scenarios.

In order to capture the wall temperature response of the heated portion, 7 axially equidistant thermocouple measuring stations ($m = 1$ to $m = 7$ in Figure 2) separated by an axial distance of $L = 0.3$ m were used. Each station consisted of 8 T-type thermocouples ($n = 1$ to $n = 8$ in Figure 3) equally spaced

around the tube circumference. The thermocouples were each positioned precisely below each heating strip. The thermocouples were installed in 3.2 mm wide grooves that were cut circumferentially around the tube to a depth of 1.77 mm before the heating strips were attached. This ensured that the thermocouples (0.5 mm in diameter) captured the stainless steel wall temperature and not the heating element temperatures. To improve thermal connectivity to the stainless steel, an epoxy with a thermal conductivity of 1.1 W/mK was used to attach the thermocouples into the grooves. Extreme caution was used to ensure that the thermocouple tip was placed on the stainless steel surface to ensure minimal influence from the thermal epoxy. The grooves also assisted with passing the thermocouple lead below the heating strips.

In order to measure the inlet and outlet bulk fluid temperatures, additional thermocouples were installed (4 each) at the inlet measuring station at $m = 0$ before the entry length and at the outlet measuring station at $m = 8$ after the heated length. These measuring stations were each equipped with flow mixers to disturb the thermal boundary layers and were thermally isolated from the test section via rubber hoses. The entire test section was also thermally insulated with 130 mm thick insulation which had an effective thermal conductivity of 0.035 W/mK.

TEST PROCEDURE

The thermocouples were calibrated *in situ* to an accuracy of 0.13 °C. Water was circulated through the system until the chiller was able to provide inlet water at a roughly constant 20°C. Depending on the test case, some, or all of the heating elements were switched on, according to the desired heat flux distribution and intensity. The power sent through to the elements was set prior to the elements being switched on. The flow was set to the highest testing condition first (Re = 2600) and was slowly decreased by roughly 150 for each interval until the lowest testing flow rate was reached (Re = 650). Before data was captured for any of the cases, steady state needed to be achieved. This was deemed to have been reached when there was less than a 0.1°C fluctuation between the difference between the average inlet and outlet temperatures, over a minute. A minimum of 200 data points were captured and logged at a frequency of 20 Hz for each case.

Heat flux case types

Three heat flux case types are considered in this paper. The first case type was that of uniform heat flux, where all the heating elements strips were powered (n=1 to n=8). This will be referred to as the 360˚ case type. The second case type was where only the bottom half of the tube was heated at local uniform heat flux intensities. This will be referred to as the bottom 180˚ case type with only elements $n = 3$ to $n = 6$ being powered. The third case was when only the top half of the tube was heated, also at local uniform heat flux intensities. Likewise this will be referred to as the top 180˚ case type with elements $n = 1,2,7,8$ being powered. A local uniform heat flux intensity of 4631 W/m² is presented in this paper. A summary of the test cases are given in Table 1 and a graphical representation of the heat flux distributions are presented in Figure 4.

Table 1 Heating degrees and corresponding active heating elements.

	Heated span	Powered heating strips	$\dot{Q}$ [W]
Case 1	360°	n =1,2,3,4,5,6,7,8	800
Case 2	Bottom 180°	n = 3,4,5,6	400
Case 3	Top 180°	n = 1,2,7,8	400

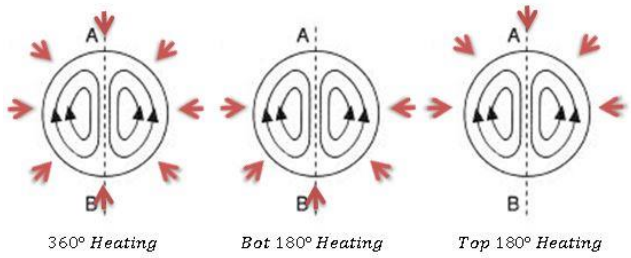

Figure 4 Heat flux distribution and secondary flow.

DATA REDUCTION METHOD

To ensure accuracy and to check that the insulation was sufficient, an energy balance was performed before continuing with the data reduction procedure. The power supplied by the power supply, $\dot{Q}_{in}$, was compared to the heat transfer rate absorbed into the water, $\dot{Q}_{out}$, in terms of the measured bulk temperatures difference:

$$\dot{Q}_{out} = \dot{m} C_p (\bar{T}_{out} - \bar{T}_{in}) \quad (1)$$

Here $\dot{m}$ was obtained from the mass flow meter and $\bar{T}_{out}$ and $\bar{T}_{in}$ were determined by taking the arithmetic average of the thermocouples at measuring stations m=8 and m=0 respectively. The specific heat value, C_p, was evaluated at the average bulk temperature within the test section. The energy balance error (% value) was calculates as follows:

$$EB = 100 \frac{\left|\dot{Q}_{in} - \dot{Q}_{out}\right|}{\frac{1}{2}\left(\left|\dot{Q}_{in}\right| + \left|\dot{Q}_{out}\right|\right)} \quad (2)$$

In this study the maximum energy balance error was 5.81% while 71.1 % of all data had an error of less than 4 %. For calculation purposes, heat rates were based on the water side heat transfer since this had a lower measuring uncertainty.

In order to determine the heat transfer coefficient, the wetted wall temperatures are needed. For this purpose, only measuring stations m=2 to m=6 were used since stations m=1 and m=7 were positioned on the edges of the heated section. They were, however used for monitoring purposes.

Since the thermocouples were installed inside the stainless steel tube wall, and since stainless steel has a relatively low

thermal conductivity, the measured thermocouple values could not be used directly to determine the wetted wall temperatures due to the significant temperature drop from the thermocouple positions in the wall to inner surface of the wall. For this purpose a semi-analytical/empirical/experimental approach was used to determine the temperature difference between each thermocouple tip and its associated wetted wall position.

Firstly, the installed radial positions of each thermocouple needed to be calibrated. This was necessary since even though the groove depth within the tube wall was relatively small, a significant temperature difference existed across it in the radial direction. Positional calibration data was collected experimentally for uniform heated conditions at high mass flow cases where it was known that secondary flow was insignificant. This allowed for the use of the well-known turbulent heat transfer coefficient correlations from literature to back-calculate the effective wetted wall temperatures from the measured inlet and outlet bulk fluid temperatures by using the recorded heat transfer rates from the heating elements. Since there was little to no secondary flow, a circumferentially uniform wall temperature could be achieved at each axial position. By comparing the measured thermocouple tip temperatures with the calculated expected wetted wall temperature, the energy balance principle was used to determine the exact radial position of each thermocouple within the grooves.

Next, an analytical model was required to determine the relative tangential heat conduction rates when non-uniform heat flux cases were considered. Even though stainless steel has a low thermal conductivity, this was needed since the thermocouple positions around the circumference was relatively close to each other. Heat input from a particular heating element was not necessarily transferred in only the radial direction, but depending on whether the neighboring heating elements were powered or not, a significant proportion of the heat could have been transferred tangentially. This was done by assuming one dimensional heat transfer. The tube was divided into 8 different sectors. The heat input was then divided evenly to the sectors where the heating was applied. Using the tangential conduction resistance, the heat input and adjacent sector temperatures, the center temperature for a specific sector could be found. The amount of heat transferred from each sector to the water was found using the temperature difference between the sector and the water, as well as the convective resistance. The percentage of the heat transferred by each sector could then be found by comparing the sector with the maximum heat input to each individual sectors heat transfer to the water. This resulted in an analytically obtained database which could be consulted for any heating element powered-on combination to determine what the effective radial heat transfer rates would be in each of the sectors (n = 1 to n =8) around the tube. Table 2 gives an example of the relative radial heat correction values when n = 3 to n = 6 are powered (bottom 180°case). From this table it can be seen that even though sectors 1, 2, 7 and 8 where not powered, a radial heat flux of between 12.3% and 26.8% of the externally applied heat flux was present due to the tangential heat conduction effect.

Combined with the calibrated thermocouple radial positions, information like this allowed for the local wetted wall temperatures to be determined from the measured thermocouple values. Once the wetted wall temperatures were obtained, the applicable average wall temperatures (local or overall) were calculated as the arithmetic average for stations m = 2 to m = 6 and sectors n = 1 to n = 8.

Table 2 Radial heat flux correction values for bottom 180°

Sector	Local radial heat flux as a percentage of the externally applied heat flux
n = 1	12.3%
n = 2	26.8%
n = 3	73.2%
n = 4	87.7%
n = 5	87.7%
n = 6	73.2%
n = 7	26.8%
n = 8	12.3%

The average temperature difference between the wall and fluid was calculated using:

$$\Delta\bar{T} = \bar{T}_w - \bar{T}_B \tag{3}$$

The effective average heat transfer coefficient was found by using the calculated heat transfer rate, the full internal tube surface area and the temperature difference.

$$h = \frac{\dot{Q}_{out}}{A_s \Delta\bar{T}} \tag{4}$$

The effective Nusselt number was based on the calculated heat transfer coefficient, the inner diameter of the tube and the thermal conductivity of the water, evaluated at the average bulk temperature.

$$Nu = \frac{hD}{k} \tag{5}$$

COMPARISON

To ensure the test setup was producing meaningful results, the captured and processed data was compared with correlations found in previous works [3, 10, 11] for uniform heat flux cases. In Figure 5 the Nusselt numbers as obtained in this investigation for an overall heat transfer rate of 800W are compared with the predictions by correlations found in literature. The experimental results include error bars of around 3.4% to account for the uncertainty in the data capturing process and the associate uncertainty propagation. Also included in the figure is the pure forced convection laminar Nusselt number of 4.36. Although the Nusselt numbers obtained in this investigation are higher than the Nusselt

numbers predicted by the correlations, the differences can be explained for each case.

In the case of Ghajar and Tam [10], which gave prediction of between 4.03% and 12.31% below the experimental heat transfer coefficients, the ranges for both the Grashoff and Prandlt numbers did not match those in this experimental results. The Grashoff range for the correlation was too low, while the Prandlt range was too high. By investigating the effects of the Grashoff and Prandlt numbers on the Nusselt number it can be shown why the experimental Nusselt numbers are higher than that of the correlations. When the Prandlt number is raised the Nusselt number increases, and when the Grashoff number is decreased the Nusselt number decreases.

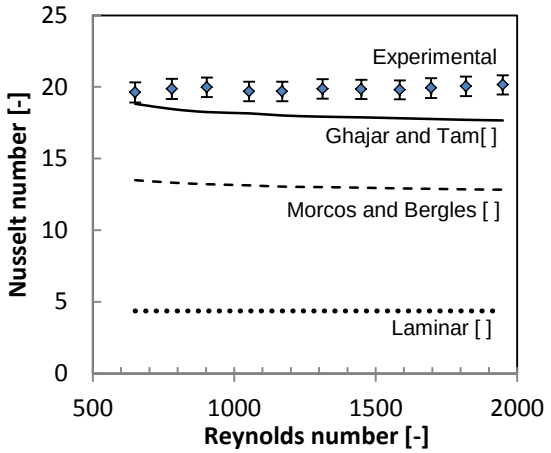

Figure 5 Comparison with literature for the 360° case.

The Grashoff number range between the experimental properties and those in the correlation differs by a factor of a hundred, whereas, the Prandlt range is only out by a factor of ten. This means that although the Prandlt number has more of an influence in the given correlation, because of the magnitude of change in the ranges in the Grashoff numbers, the Nusselt number decreases when the actual ranges are used for the correlation case.

When considering the Morcos and Bergles case, the difference is that their conditions where for fully developed flow, both hydrodynamically and thermally while in this paper the flow is only thermally developing. Therefore, the development of the thermal profile could be the reason why the Nusselt number in this paper is larger than that of Morcos and Bergles.

TRENDS AND RESULTS

The Nusselt number results are contained in Figure 7 for the top and bottom 180° cases, as well as the 360° case. It can be seen that the Nusselt numbers are lower in the 180° cases when compared to the 360° case. The Nusselt numbers of the top 180° case were the lowest.

It was seen that the Nusselt numbers for the top and bottom 180° cases merged at around Re = 2600. The reason for this could be due to the relative magnitude of the secondary flow for the different cases. This would mean that the flow becomes purely forced around this region, or at least having the same amount of mixed convection. If the flow is purely forced, the effect of the gravity, and therefore the buoyancy forces, becomes less significant and therefore the top and bottom heating cases could be expected to become more identical. The Nusselt numbers for the 360° case remain almost constant throughout the Reynolds number range. There is a 9.1% decrease between the Nusselt numbers at a low Reynolds number to those at a high Reynolds number for the bottom 180°case. There is a 9.2% increase between the Nusselt numbers at a low Reynolds number to those at a high Reynolds number for the top 180°case. When the two 180° cases merge at Re = 2600, the difference between those Nusselt numbers and the Nusselt numbers for the 360°case at the same Reynolds number is 18.26%.

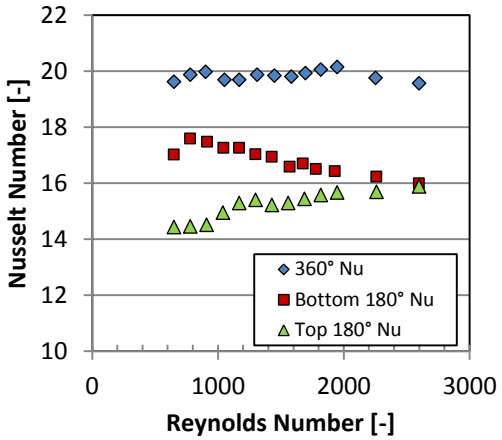

Figure 6 Nusselt number comparisons for both the 180° and the 360° cases.

Table 3 gives a sample of the wall temperature data for the different cases (360° and both 180° cases) at a Reynolds number of 1300. The Reynolds number and heat transfer rate are only selected as an example in order to show the effect of the change between the different applied heat flux configurations. The colour scales give a better indication of the temperature profile present in the tube for the different cases.

Table 3 Example data for the wetted wall temperatures for Re = 1300

Case 1, 360°					
n	***m* = 6**	***m* = 5**	***m* = 4**	***m* = 3**	***m* = 2**
1	47.39	44.91	43.61	41.35	38.88
2	39.38	35.45	34.62	33.99	32.22
3	34.11	31.99	31.47	31.19	30.49
4	31.21	30.00	29.92	29.85	29.62
5	31.19	30.11	29.98	29.82	29.67
6	34.27	32.91	31.81	31.66	30.69
7	38.72	37.08	35.14	34.25	32.71
8	46.82	45.05	43.32	41.89	38.95
Case 2, Bottom 180°					
1	27.22	26.19	25.32	25.69	24.80
2	28.65	27.50	27.01	27.04	26.27
3	30.71	29.45	29.31	29.29	29.30

4	30.89	30.22	30.03	31.80	30.19
5	31.49	30.52	31.20	29.71	30.27
6	31.49	29.52	29.62	29.78	28.81
7	29.08	27.99	28.22	27.92	27.11
8	27.43	26.73	25.65	25.54	24.91
Case 3, Top 180°					
1	42.53	41.08	40.53	38.69	36.82
2	33.47	30.63	29.84	30.08	29.15
3	25.45	24.41	24.06	24.55	24.02
4	22.11	21.60	21.87	23.01	21.77
5	22.56	22.20	21.57	21.39	21.81
6	25.87	26.47	24.34	23.91	23.98
7	33.50	33.19	30.28	29.61	28.72
8	42.45	41.25	39.89	39.14	36.88

Figure 7 shows the relative axial average wall temperatures difference to the fluid temperature. The figure gives a good representation of the effect the incoming heat flux has on the local wetted wall temperatures, and what effect it has on the fluid flow within the tube. It can be seen that there is a marked difference between the circumferential wall temperatures when comparing the 360° and 180° cases. The top of the tube (n = 1 and n = 8) is seen to be hotter in the 360° case, which is expected due to the buoyancy of the fluid. This is intensified in the top 180° case. The reason for the higher Nusselt numbers for the 360° case is due the measured higher temperature difference. In general it can be expected that buoyancy forces cause the warmer fluid to move to the top of the tube while the main fluid flow continues through the tube. With warmer temperatures present at the bottom of the tube as can be seen in Figure 7 for the bottom 180° heating case, there would be a larger buoyancy force which in turn would create larger relative magnitude of secondary flow and cause higher Nusselt numbers for that heating case. For the top 180° case the opposite is true and warm water is trapped at the top of the tube.

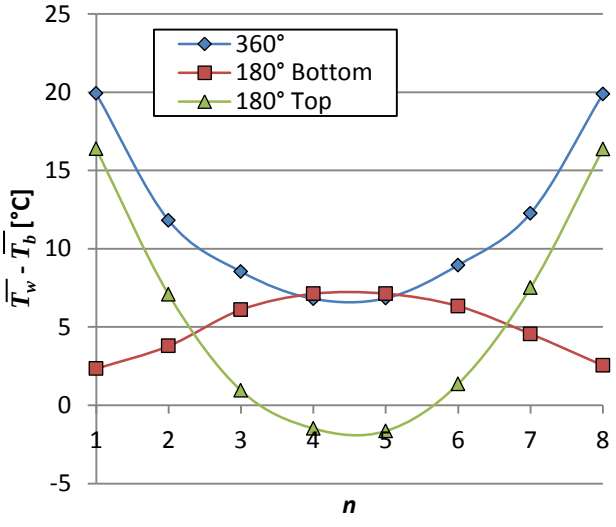

Figure 7 Wall temperatures at m = 6, with Re = 1300

CONCLUSION

In this paper the influence of different externally applied heat flux distributions on the effective average internal Nusselt number is considered in the laminar flow regime for a 2 m long stainless steel tube with an inner diameter of 27.8 mm and a wall thickness of 2.77 mm. The three heat flux distributions, 360° fully uniform and 180° top and bottom half locally uniform heat flux cases resulted in significant differences in the average circumferential wall temperature profiles and effective overall internal heat transfer coefficient. The 360° case produced the highest Nusselt numbers followed by the bottom 180° case. The top 180° case produced the lowest Nusselt number. Due to the effect of buoyancy driven secondary flow all cases produced significantly higher Nusselt number values than that of a pure forced convection case. For the 360° case the Nusselt number remained approximately constant over the full range of Reynolds numbers, while for the 180° bottom and top cases, the Nusselt numbers reduced and increased respectively as the Reynolds number increased. At a Reynolds number of approximately 2600, there was no notable difference in the top and bottom 180° cases. Further work is needed to investigate the effect of among others, the local heat flux intensities.

REFERENCES

[1] Concentrating solar power: its potential contribution to a sustainable energy future. *The European Academies Science Advisory Council (EASAC) policy report 16*.

[2] Chang, C., X. Li, and Q.Q. Zhang, Experimental and Numerical Study of the Heat Transfer Characteristics in Solar Thermal Absorber Tubes with Circumferentially Non-uniform Heat Flux. *Energy Procedia*, 2014. 49(0): pp. 305-313.

[3] Cengel, Y.A., Heat and Mass Transfer: A Practical Approach, 3rd Edition (SI Units)2006, New York: McGraw-Hill. pp. 530-531.

[4] Kakaç, S., R.K. Shah, and W. Aung, Handbook of single-phase convective heat transfer1987: Wiley New York et al. pp. 15.1-15.27.

[5] Bergles, A. and R. Simonds, Combined forced and free convection for laminar flow in horizontal tubes with uniform heat flux. *International Journal of Heat and Mass Transfer*, 1971. 14(12): pp. 1989-2000.

[6] Kupper, A., E. Hauptmann, and M. Iqbal, Combined free and forced convection in a horizontal tube under uniform heat flux. *Solar Energy*, 1969. 12(4): pp. 439-446.

[7] Mohammed, H.A. and Y.K. Salman, Experimental investigation of mixed convection heat transfer for thermally developing flow in a horizontal circular cylinder. *Applied thermal engineering*, 2007. 27(8): pp. 1522-1533.

[8] Mohammed, H.A. and Y.K. Salman, Free and forced convection heat transfer in the thermal entry region for laminar flow inside a circular cylinder horizontally oriented. *Energy Conversion and Management*, 2007. 48(7): pp. 2185-2195.

[9] Patankar, S., Numerical heat transfer and fluid flow1980: CRC press. pp.

[10] Ghajar, A.J. and L.-M. Tam, Heat transfer measurements and correlations in the transition region for a circular tube with three different inlet configurations. *Experimental thermal and fluid science*, 1994. 8(1): pp. 79-90.

[11] Morcos, S. and A. Bergles, Experimental investigation of combined forced and free laminar convection in horizontal tubes. *Journal of Heat Transfer*, 1975. 97(2): pp. 212-219.